


 Cite this: *RSC Adv.*, 2026, 16, 2417

Design, synthesis and evaluation of new pyrazino [1',2':1,5]pyrrolo[2,3-*d*]pyrimidines as tacrine-like acetylcholinesterase inhibitors

Liubov V. Muzychka, * Oksana V. Muzychka, Oleksandr L. Kobzar, Andriy I. Vovk and Oleg B. Smolii

The development of acetylcholinesterase (AChE) inhibitors remains a promising research direction in drug discovery for Alzheimer's disease. A series of eighteen pyrazino[1',2':1,5]pyrrolo[2,3-*d*]pyrimidine derivatives was synthesized as novel tacrine-like AChE inhibitors. Sixteen compounds inhibited AChE in the micromolar range. Among them, 4-(dimethylamino)-7,8-dimethylpyrazino[1',2':1,5]pyrrolo[2,3-*d*]pyrimidin-6(*7H*)-one (**22**) exhibited the highest inhibitory activity against the enzyme with an IC₅₀ value of 0.22 ± 0.02 μM, showing mixed-type inhibition. *In silico* studies showed that **22** occupies the catalytic anionic site of hAChE and forms strong π–π stacking interactions with Trp86, similar to those of tacrine. This study demonstrates the potential use of methyl-substituted pyrazino[1',2':1,5]pyrrolo[2,3-*d*]pyrimidines in the development of potent AChE inhibitors.

 Received 5th September 2025
 Accepted 29th December 2025

DOI: 10.1039/d5ra06700f

rsc.li/rsc-advances

Introduction

Alzheimer's disease (AD) is a progressive neurodegenerative brain disorder that causes memory loss, cognitive decline, and abnormal behaviour.^{1–3} Acetylcholine deficiency is a key contributor to the cognitive symptoms of AD. Cholinesterase inhibitors are used to alleviate the symptoms of neurological diseases and improve cognitive function in patients with AD.^{4,5} Currently, there are four FDA-approved acetylcholinesterase (AChE) inhibitors, donepezil, rivastigmine, galantamine, and benzgalantamine, that lead to increased acetylcholine levels in the synaptic cleft. Together with memantine, the *N*-methyl-*D*-aspartate antagonist, they constitute all the approved small-molecule drugs for the treatment of AD.^{2,6–9} However, these drugs have suboptimal pharmacokinetics and pharmacodynamics and may cause gastrointestinal tract disorders.^{10–12} Due to concerns about their toxicity and side effects, there is a growing interest in developing better treatments for AD through the structural optimisation of existing drug scaffolds.⁶

Heterocyclic compounds have played a significant role in the discovery of potent cholinesterase inhibitors.^{13–18} Tacrine was the first AChE inhibitor approved for the treatment of AD, but it was withdrawn from the market due to its hepatotoxicity and poor therapeutic efficacy.¹⁹ Despite its limitations, the tacrine scaffold remains an attractive starting point for the development of new AChE inhibitors with improved pharmacological profiles.^{20–22} Indeed, most tacrine derivatives exhibit high AChE inhibitory activity and lower toxicity.^{23–26} Many tacrine-like

tricyclic compounds have been designed and tested against AChE. In particular, thiazolo[5',4':4,5]pyrimido[1,2-*a*]azepinones, tetrahydropyridothienopyrimidinones, cyclohepta[*b*]thieno-oxazines, 1,2,3-triazolo[4,5-*b*]aminoquinolines, pyrrolo[2,1-*b*]quinazolin-9(*1H*)-ones, and pyrido[1,2-*a*]thiazolo[5,4-*d*]pyrimidinones inhibited AChE in the micromolar range.^{27–32} Notably, pyrazino[1,2-*a*]indol-1(*2H*)-one, tetrahydrobenzo[1,8-*b*]naphthyridine, and pyrazolo[1,2-*b*]phthalazine derivatives showed nanomolar IC₅₀ values.^{33–35} Overall, replacing the benzene ring in the tacrine structure with various heterocyclic systems contributed to high anticholinesterase activity and selectivity.^{6,27,30–35}

We recently reported the synthesis and evaluation of 4,7-substituted 8,9-dihydropyrazino[1',2':1,5]pyrrolo[2,3-*d*]pyrimidine derivatives. The studied compounds containing different alkyl, dimethylaminoalkyl, or methoxy substituents at positions 4 and 7 demonstrated promising inhibitory activity against AChE.³⁶ In addition, the tricyclic thienopyrimidinone²⁸ and indol-1(*2H*)-one³³ derivatives showed effective inhibition of AChE, enhanced by non-polar substituents at positions 7 and 8. Inspired by these results, we present the design and synthesis of eighteen new tacrine-like AChE inhibitors with a pyrazino [1',2':1,5]pyrrolo[2,3-*d*]pyrimidine core (Fig. 1). We explored two series with a dihydropyrazine (structure **A**) or a pyrazine ring (structure **B**) and introduced methyl substituents at positions 4, 7, and 8 to study the structure–activity relationship. We hypothesized that the addition of methyl groups would provide additional hydrophobic interactions, while modification of the azatricyclic system with amino groups would lead to more efficient hydrogen bonding with key tyrosine residues at the AChE active site. The synthesized compounds were evaluated *in vitro*

V.P. Kukhar Institute of Bioorganic Chemistry and Petrochemistry, NAS of Ukraine, 1 Academic Kukhar Str., Kyiv 02094, Ukraine. E-mail: liubovmuzychka@gmail.com



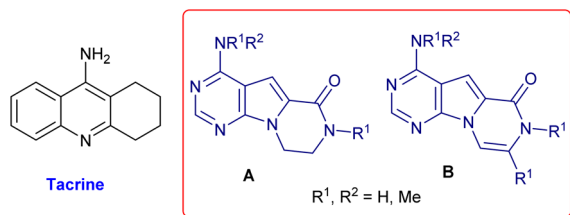


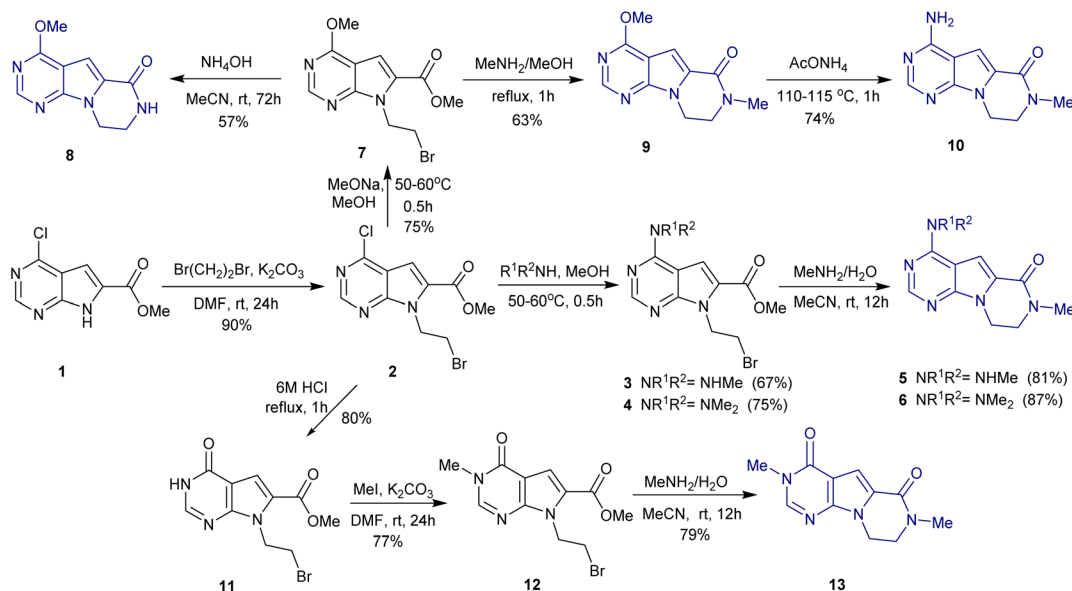
Fig. 1 Structures of tacrine and target pyrazino[1',2':1,5]pyrrolo[2,3-d]pyrimidine derivatives.

for their inhibitory activity against AChE. The binding of the most potent compound was further investigated by kinetic analysis, molecular docking, and molecular dynamics simulations. Its cytotoxicity was also studied in a hepatocellular carcinoma cell line HepG2. Additionally, ADMET properties of the synthesized compounds were predicted *in silico* to assess their drug-likeness.

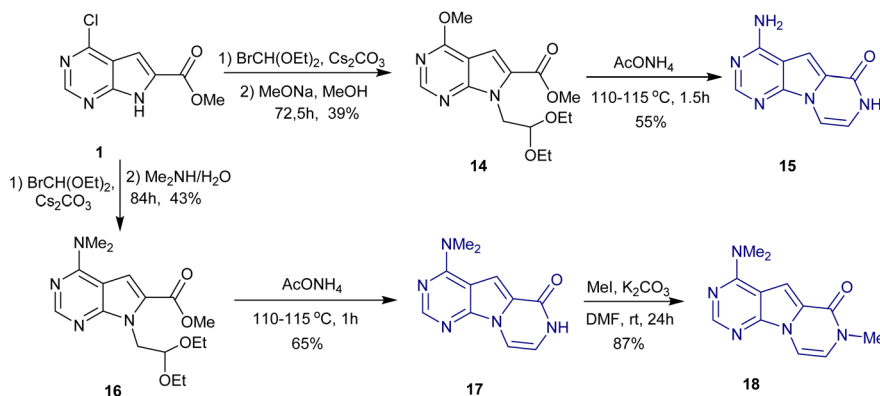
Results and discussion

Chemistry

The synthesis of 8,9-dihydropyrazino[1',2':1,5]pyrrolo[2,3-d]pyrimidines **5**, **6**, **8–10**, and **13** was completed in three or four steps, depending on the substitution at positions 3 and 7 (Scheme 1). Methyl 4-chloro-7H-pyrrolo[2,3-d]pyrimidine-6-carboxylate **1** was used as the starting material to synthesize the intermediates **3**, **4**, and **7** in two steps, as previously reported.³⁶ 3-Substituted derivative **12** was prepared from **2** *via* reflux in 6 M hydrochloric acid, followed by methylation with methyl iodide in dimethylformamide in the presence of K₂CO₃.³⁶ The formation of the dihydropyrazine ring was the last step of the synthesis of the target compounds **5**, **6**, **8**, **9**, and **13**. It was accomplished by treating compounds **3**, **4**, **7**, and **12** with excess aqueous ammonia or methylamine at room temperature or by refluxing **7** with methylamine solution in MeOH. Heating of **9** with ammonium acetate gave the target 4-amino-substituted derivative **10**.

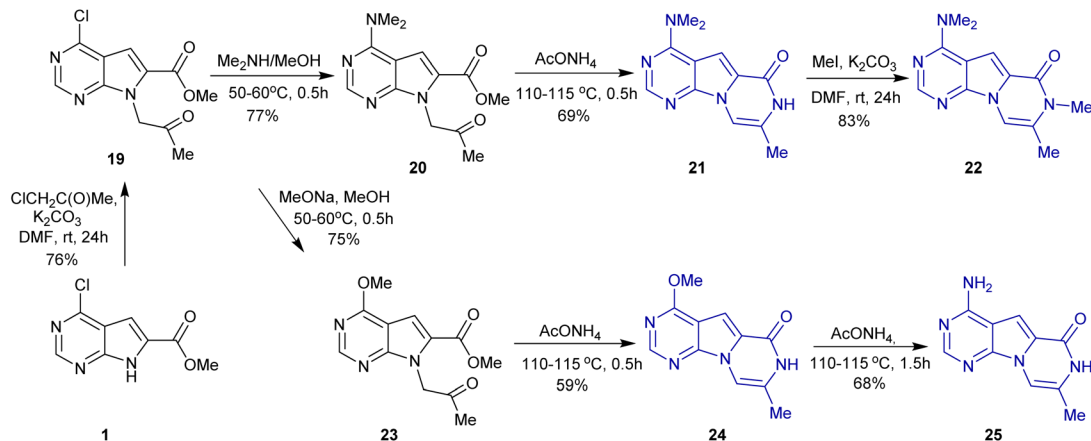


Scheme 1 Synthesis of the target 8,9-dihydropyrazino[1',2':1,5]pyrrolo[2,3-d]pyrimidines **5**, **6**, **8–10**, and **13**.



Scheme 2 Synthesis of the target pyrazino[1',2':1,5]pyrrolo[2,3-d]pyrimidines **15**, **17**, and **18**.





Scheme 3 Synthesis of the target pyrazino[1',2':1,5]pyrrolo[2,3-d]pyrimidine derivatives 21, 22, 24, and 25.

Analogs 15, 17, and 18 containing a pyrazine ring were also synthesized from carboxylate 1 (Scheme 2). Alkylation of 1 and subsequent nucleophilic substitution with sodium methoxide or dimethylamine gave key intermediates 14 and 16. Then, 15 and 17 were prepared *via* treatment with ammonium acetate, which mediated pyrazine ring formation and the conversion of the methyl ether of 15 to the amino group at position 4. Methylation of 17 afforded the target compound 18.

A new efficient synthetic approach was developed to introduce a methyl group at position 8 and to prepare derivatives 22 and 25 (Scheme 3). The key intermediate 19 was obtained by the alkylation of 1 with chloroacetone. Then, 22 was synthesized from 19 *via* three steps: nucleophilic substitution, cyclization, and methylation. Alternatively, 19 was treated with sodium methoxide in methanol to convert the chloride into the ether 23. The reaction of 23 with ammonium acetate yielded both 24 and 25, depending on the reaction time (Scheme 3). Functionalization of 24 afforded three more derivatives 26, 27, and 28 (Scheme 4).

Additionally, 3-methyl substituted pyrazino[1',2':1,5]pyrrolo[2,3-d]pyrimidine 33 was prepared in four steps (Scheme 5). The

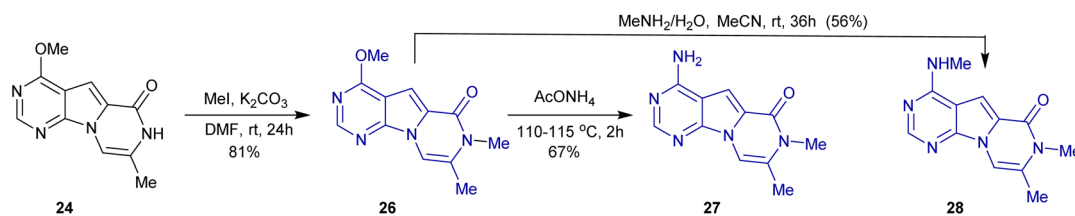
starting material iodomethylpyrimido[5',4':4,5]pyrrolo[2,1-c][1,4]oxazine 29 was obtained according to the previously reported procedures.^{37,38} Methylation of 29 and iodine elimination with sodium acetate gave the alkene intermediate 31. Upon treatment with ammonium acetate, the oxazine ring was converted into a pyrazine, and methylation of 32 gave 33 in a high yield.

The structures of the synthesized compounds were confirmed by the elemental analysis, ¹H and ¹³C NMR spectroscopy, and mass spectrometry.

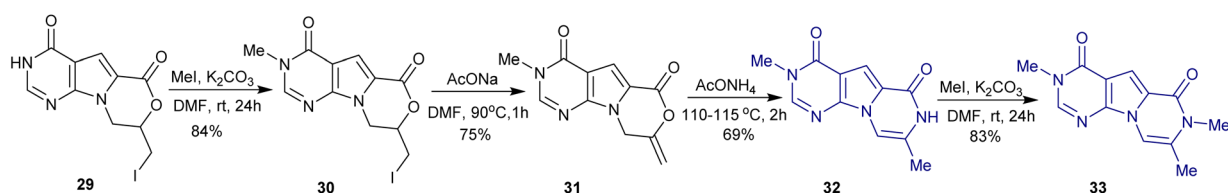
Acetylcholinesterase inhibition

The inhibitory activity of pyrazino[1',2':1,5]pyrrolo[2,3-d]pyrimidine derivatives against AChE from electric eel was tested *in vitro* using a modified Ellman's method.³⁹ The studied compounds inhibited AChE with IC₅₀ values ranging from >100 to 0.22 μM (Table 1).

A structure–activity relationship study indicates that the presence of a pyrazine moiety in the inhibitor structures increases their potency compared to the compounds with



Scheme 4 Synthesis of the target compounds 26–28.



Scheme 5 Synthesis of pyrazino[1',2':1,5]pyrrolo[2,3-d]pyrimidine derivatives 32 and 33.



Table 1 Inhibition of AChE by the synthesized pyrazino[1',2':1,5]pyrrolo[2,3-d]pyrimidines. ^a

Compound	IC ₅₀ , μM
5	15.86 ± 1.58
6	7.17 ± 1.01
8	>100
9	78.93 ± 12.57
10	77.87 ± 3.02
13	14.92 ± 0.51
15	>100
17	12.03 ± 0.91
18	2.43 ± 0.26
21	1.03 ± 0.08
22	0.22 ± 0.02
24	6.23 ± 1.53
25	15.84 ± 1.26
26	0.61 ± 0.14
27	0.46 ± 0.02
28	0.61 ± 0.11
32	14.26 ± 1.73
33	1.24 ± 0.31
Donepezil ^b	0.016 ± 0.001
Tacrine ^b	0.054 ± 0.001

^a IC₅₀ values are shown as the average value ± standard deviation.

^b Reference compound.

a dihydropyrazine fragment (5, 6, 8–10, and 13). The methyl group at position 7 of the pyrazino[1',2':1,5]pyrrolo[2,3-d]pyrimidine core also played an important role in the enzyme inhibition. Compounds 9, 18, 22, 26, 27, and 33 exhibited higher inhibitory activity than their respective unsubstituted analogs 8, 17, 21, 24, 25, and 32. Similarly, methyl substitution at position 8 led to a significant improvement in the potency of 21, 22, and 25 compared to their unsubstituted derivatives 17, 18, and 15. Overall, a dimethylamino group at position 4 was more favorable for AChE inhibition than (methyl)amino, methoxy, or methylamide moieties, as is evident when comparing IC₅₀ values of compounds 22, 28, 27, 26, and 33. These results demonstrate that methyl substituents can enhance inhibitor binding affinity to AChE.

Among the synthesized compounds, 4-(dimethylamino)-7,8-dimethylpyrazino[1',2':1,5]pyrrolo[2,3-d]pyrimidin-6(7H)-one (22) was the most potent AChE inhibitor, showing an IC₅₀ value of 0.22 ± 0.02 μM. Kinetic studies were performed to elucidate the mechanism of the enzyme inhibition. A Lineweaver–Burk plot (Fig. 2) showed mixed-type inhibition, indicating that the inhibitor can bind to both the free enzyme and the enzyme–substrate complex. The calculated K_i and K_i' values are 0.207 ± 0.05 μM and 0.343 ± 0.07 μM, respectively.

All tested compounds were also evaluated *in vitro* for their activity against butyrylcholinesterase from equine serum. However, no inhibitory effect was observed at a concentration of 10 μM.

Molecular docking

To simulate interactions between the enzyme and the inhibitor, compound 22 was docked to human acetylcholinesterase

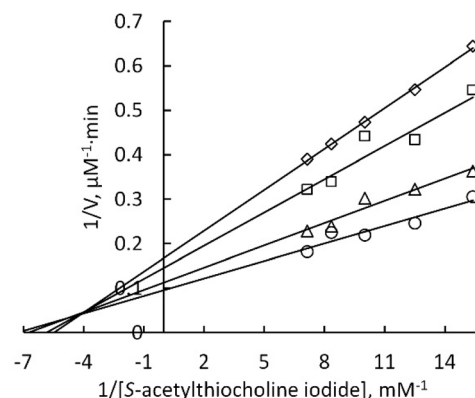


Fig. 2 Lineweaver–Burk plot for inhibition of AChE by compound 22. The concentrations of the inhibitor were 0 (○), 70 nM (△), 140 nM (□), and 280 nM (◇).

(hAChE) using AutoDock Vina software.⁴⁰ The human enzyme shares conserved amino acid residues of the active site and has remarkable homology with the AChE obtained from the electric eel.⁴¹ Molecular docking, which sheds light on intermolecular interactions between the inhibitor and the enzyme, is considered a pivotal technique in the rational design of AChE inhibitors.⁴² The crystal structure with PDB code 7XN1 ref. 43 was used for docking. The tacrine molecule in the anionic subsite of the enzyme's catalytic site (CAS) was removed before calculations. First, a blind docking calculation to the entire surface of hAChE was performed to identify the inhibitor binding sites. The results showed that compound 22 is capable of occupying the CAS as well as the peripheral anionic site (PAS), located at the entrance to the catalytic gorge. Although ligand positioning at the PAS was observed more frequently, the CAS location was approximately 1 kcal mol⁻¹ more favorable. The docking was repeated 18 times, and the binding poses with the lowest docking energies were analyzed.

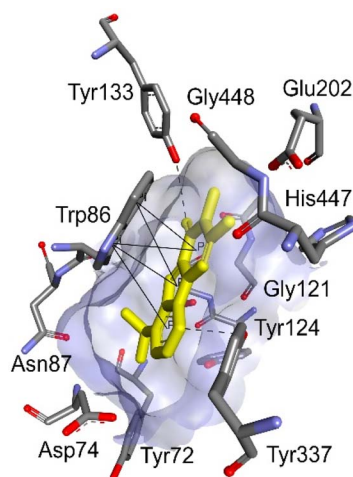


Fig. 3 Binding mode of compound 22 in the CAS of hAChE predicted by molecular docking calculations. Hydrogen atoms of the amino acid residues are hidden.



Based on these data, compound **22** was specifically docked into the anionic subsite of the CAS. When occupying the anionic subsite (Fig. 3; calculated docking energy was -8.5 kcal mol $^{-1}$), the pyrazino[1',2':1,5]pyrrolo[2,3-*d*]pyrimidine scaffold of the inhibitor forms multiple π - π stacking contacts with the indole ring of Trp86, similar to those of tacrine in the crystal structure PDB 7XN1. The pyrazinone and pyrimidine rings of the ligand have hydrogen bonds with Tyr133 and Tyr337 through the keto group and nitrogen atom, respectively. The dimethylamino group of the inhibitor is directed to Tyr72. Additionally, the binding pose of compound **22** within the CAS of hAChE is stabilized by electrostatic and van der Waals interactions with surrounding amino acid residues.

Molecular dynamics simulations

Molecular dynamics (MD) simulations were performed to better understand the intermolecular interactions in the hAChE-inhibitor complex. Studies of the hAChE-tacrine complex (co-crystallized ligand) were carried out to validate the molecular dynamics calculation protocols and to compare these results with those obtained for compound **22**. As shown in Fig. 4A, the time-dependent changes in the root mean square deviation (RMSD) of the protein backbone atoms for studied complexes were similar and have average values \pm standard deviation of 1.235 ± 0.132 Å for free hAChE, 1.402 ± 0.216 Å for hAChE with compound **22** located in the CAS, and 1.271 ± 0.154 Å for hAChE with tacrine located in the CAS. Despite the slight RMSD perturbation observed for the hAChE-**22** complex, the studied

model systems reach equilibration approximately after 10 ns of the calculation. The root mean square fluctuation (RMSF) analysis shown in Fig. 4B demonstrates that the bound ligands only slightly change the fluctuations of the surrounding amino acid residues. The time-dependent changes in the radius of gyration (R_g), shown in Fig. 4C, indicate that the overall structural compactness of the free hAChE and its complexes with inhibitors was maintained throughout the simulation. The solvent-accessible surface area (SASA) values (Fig. 4D) showed moderate fluctuations, reflecting minor conformational flexibility of the protein while preserving its overall structural integrity. These combined results supported the conclusion that the model systems remained stable throughout the molecular dynamics simulation and were suitable for further analysis.

The binding mode of compound **22** in the CAS of hAChE, obtained at the last frame of MD simulations, is shown in Fig. 5. As can be seen, the inhibitor maintains its position relative to the docking results. Notably, the minor non-planarity of the pyrazino[1',2':1,5]pyrrolo[2,3-*d*]pyrimidine scaffold is caused by the nitrogen atom at position 10 being parameterized as a pyramidal trigonal nitrogen, which adopts a pyramidal rather than planar configuration under the applied force field during the MD simulation. The dimethylamino group adopts a planar geometry during the MD simulation, in contrast to its pyramidal shape observed in the docking calculation. This is attributed to the difference in the force fields used in docking and MD simulations.

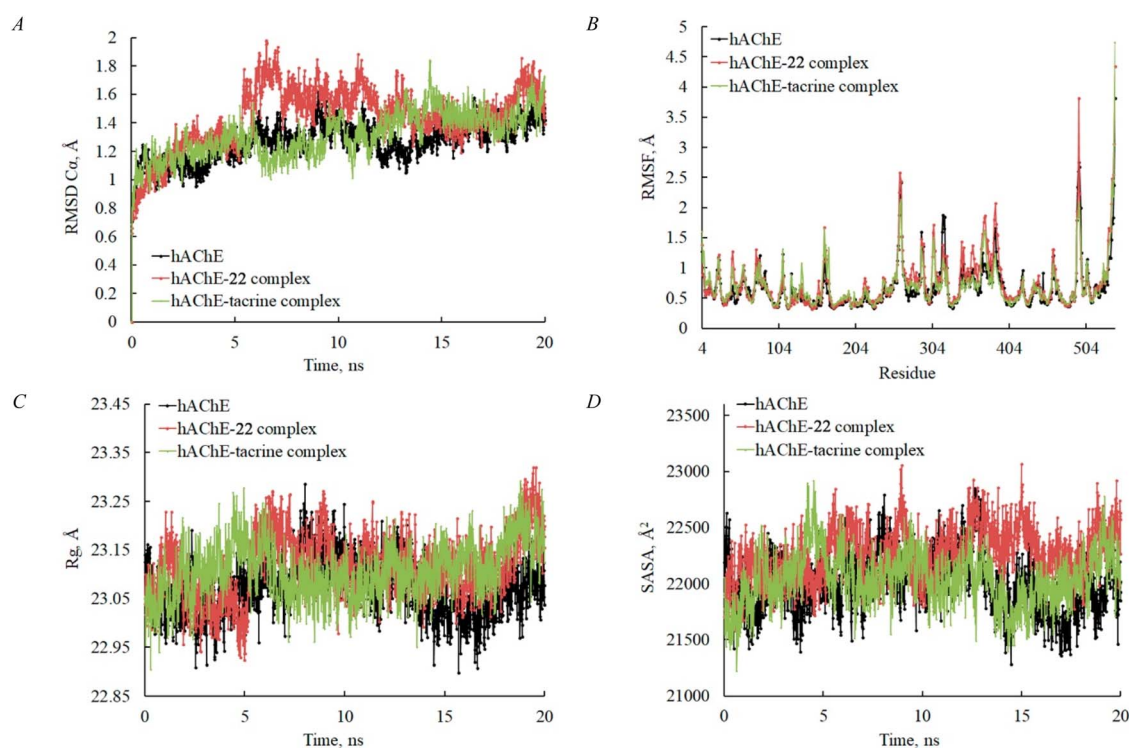


Fig. 4 Molecular dynamic analysis of the studied systems: (A) root mean square deviation (RMSD) of protein backbone atoms indicating structural stability; (B) root mean square fluctuation (RMSF) showing residue-level flexibility; (C) radius of gyration (R_g) representing protein compactness; (D) solvent accessible surface area (SASA) reflecting protein surface exposure.



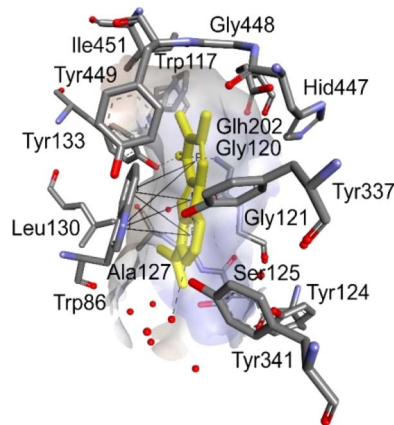


Fig. 5 Binding mode of compound 22 in the CAS of hAChE after MD simulation. The oxygen atoms of water molecules are represented as the red spheres, while the hydrogen atoms of the amino acid residues and water molecules are hidden.

Table 2 Estimated binding free energies \pm std. dev. (kcal mol⁻¹) and their MM/GBSA components for hAChE with compound 22 and tacrine located in the CAS of hAChE^a

MM/GBSA component	Compound 22	Tacrine
VDWAALS	-42.46 \pm 3.08	-31.58 \pm 2.34
EEL	-26.58 \pm 2.81	-194.59 \pm 8.41
EGB	39.10 \pm 1.93	202.16 \pm 6.70
ESURF	-4.14 \pm 0.10	-3.51 \pm 0.12
ΔG_{gas}	-69.04 \pm 3.19	-226.18 \pm 8.42
ΔG_{solv}	35.85 \pm 1.91	198.65 \pm 6.68
ΔG_{total}	-33.18 \pm 2.21	-27.52 \pm 3.00

^a VDWAALS is a van der Waals energy describing non-covalent dispersion interactions between the ligand and the enzyme in the gas phase; EEL is the electrostatic energy showing coulombic interactions between the ligand and enzyme in the gas phase; EGB polar solvation energy represents the desolvation penalty upon complex formation, estimated using the Generalized Born (GB) model; ESURF is nonpolar solvation energy approximated based on the solvent-accessible surface area (SASA), accounting for hydrophobic contributions; ΔG_{gas} is total interaction energy in the gas phase; ΔG_{solv} is total solvation energy (polar and nonpolar contributions); ΔG_{total} is the free binding energy of the complex formation.

The MM/GBSA method was employed to estimate the binding free energies and their contributing components for the enzyme-inhibitor complexes. Calculated data shown in Table 2 suggest that van der Waals (VDWAALS) and electrostatic (EEL) energies contribute to stabilization of the enzyme-inhibitor complexes, while polar solvation energy (EGB) leads to destabilization. The ΔG_{total} values indicate favorable binding in complexes.

The per-residue decomposition of the binding free energies for amino acid residues located within 4 Å of the ligands in the complexes, calculated using the MM/GBSA method, is presented in Fig. 6. According to the results, the interactions of compound 22 with Trp86, Tyr133, and Tyr337, as well as those of tacrine with Trp86 and His447, which were identified in the docking binding modes, remained stable throughout the MD simulation. These interactions were among the strongest observed and are likely responsible for stabilizing the enzyme-inhibitor complexes.

In silico ADMET prediction

The drug-like properties of the pyrazino[1',2':1,5]pyrrolo[2,3-*d*]pyrimidine derivatives were evaluated based on the *in silico* ADMET predictions. The physicochemical and ADMET characteristics of the compounds were calculated using the SwissADME web tool and the Deep-PK.^{44,45} It was found that all the pyrazino[1',2':1,5]pyrrolo[2,3-*d*]pyrimidine inhibitors of AChE fully comply with Lipinski's rule of five.⁴⁶ Compared to tacrine, new derivatives have higher molecular weight, lower log *P* values, a slightly larger number of H-bond acceptors, and greater topological polar surface area (TPSA) (Table 3). The TPSA values are below 90 Å, suggesting that the compounds may be able to cross the blood-brain barrier.⁴⁷ This assumption is further supported by the categorical model results obtained from the Deep-PK (Table 3). However, the calculated log PS values indicate only moderate penetration into the central nervous system. According to log PS values, as well as the BOILED-Egg model obtained from the SwissADME server, compound 22, which was the most potent AChE inhibitor, has a higher probability of blood-brain barrier penetration compared to the other tested pyrazino[1',2':1,5]pyrrolo[2,3-*d*]

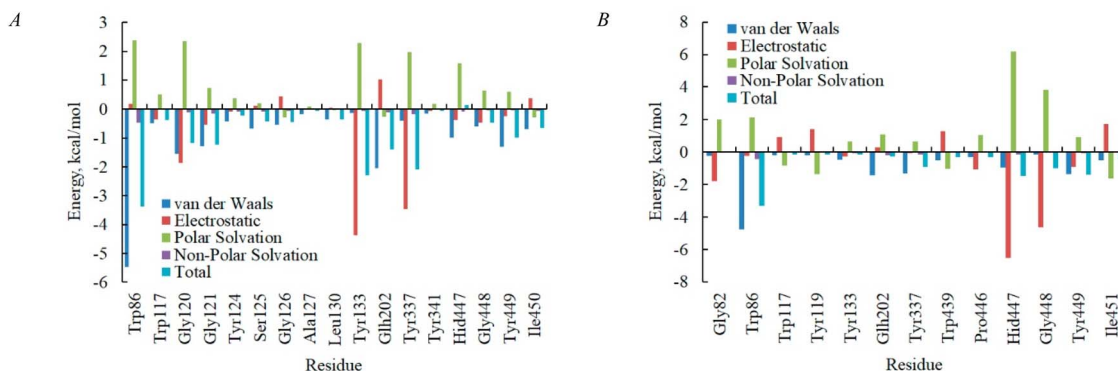


Fig. 6 Per-residue decomposition of the binding free energies for amino acid residues within 4 Å of the ligand in the hAChE-inhibitor complexes: (A) compound 22 located in the CAS of hAChE; (B) tacrine located in the CAS of hAChE.



Table 3 Calculated physicochemical parameters and pharmacokinetic properties of the pyrazino[1',2':1,5]pyrrolo[2,3-*d*]pyrimidines

Compound	MW, g mol ⁻¹	Log <i>P</i> (WLOGP)	H-bond acceptors	H-bond donors	TPSA, Å	Caco-2 permeability, log Paap (cm s ⁻¹)	Blood-brain barrier (CNS), log PS	Blood-brain barrier	Liver injury I	Liver injury II
5	231.25	-0.01	3	1	63.05	-4.54	-2.47	Penetrable	Toxic	Toxic
6	245.28	0.20	3	0	54.26	-4.58	-2.01	Penetrable	Toxic	Toxic
8	218.21	-0.20	4	1	69.04	-4.8	-3.07	Penetrable	Toxic	Toxic
9	202.21	0.14	3	0	51.02	-4.58	-2.38	Penetrable	Toxic	Toxic
10	217.23	-0.27	3	1	77.04	-4.82	-2.42	Penetrable	Toxic	Toxic
13	232.24	-0.56	3	0	60.13	-4.77	-2.52	Penetrable	Toxic	Toxic
15	203.20	-0.62	3	2	85.83	-4.99	-2.51	Penetrable	Toxic	Toxic
17	229.24	0.64	3	1	66.29	-4.82	-2.53	Penetrable	Safe	Toxic
18	243.26	0.65	3	0	55.43	-4.66	-2.31	Penetrable	Safe	Toxic
21	243.26	0.95	3	1	66.29	-4.82	-2.37	Penetrable	Safe	Toxic
22	257.29	0.96	3	0	55.43	-4.73	-2.10	Penetrable	Safe	Toxic
24	230.22	0.89	4	1	72.28	-4.83	-3.17	Penetrable	Safe	Toxic
25	215.21	0.47	3	2	89.07	-5.06	-2.58	Penetrable	Safe	Toxic
26	244.25	0.90	4	0	61.42	-4.79	-2.85	Penetrable	Safe	Toxic
27	229.24	0.48	3	1	78.21	-4.88	-2.34	Penetrable	Safe	Toxic
28	243.26	0.74	3	1	64.22	-4.81	-2.35	Penetrable	Safe	Toxic
32	232.24	-0.51	3	1	68.92	-4.96	-2.71	Penetrable	Toxic	Toxic
33	244.25	0.19	3	0	61.30	-4.83	-2.57	Penetrable	Toxic	Toxic
Tacrine	198.26	2.70	1	1	38.91	-4.71	-1.97	Penetrable	Safe	Toxic

pyrimidines, except for compound **6**. The calculated log Paap values predict that all AChE inhibitors exhibit high Caco-2 cell permeability, suggesting good intestinal mucosal absorption. Similar to tacrine, the studied pyrazino[1',2':1,5]pyrrolo[2,3-*d*]pyrimidine derivatives are predicted to have a risk of drug-induced liver injury. Overall, the *in silico* ADMET profiles of these compounds are comparable to those of tacrine.

Evaluation of cytotoxicity of **22** on the HepG2 cell line

To evaluate the hepatotoxicity of **22** as the most active compound in the series, we tested its effect on the cell viability of the human hepatocellular carcinoma cell line HepG2. HepG2 cells were exposed to the compound for 48 hours, followed by the resazurin assay to determine cell viability. The IC₅₀ for compound **22** was calculated from the top plateau at 56.4% inhibition of cell viability. The obtained IC₅₀ value was 34.5 μM, indicating moderate liver cytotoxicity (1 μM < IC₅₀ < 100 μM).

Experimental

Chemistry

¹H and ¹³C NMR spectra were obtained on Varian Unity INOVA 400 or Bruker Avance DRX-500 spectrometers in CDCl₃ [residual CHCl₃ (δ_H = 7.26 ppm) or CDCl₃ (δ_C = 77.16 ppm) as internal standard] or DMSO-*d*₆ [residual SO(CD₃)(CD₂H) (δ_H = 2.50 ppm) or SO(CD₃)₂ (δ_C = 39.52 ppm) as internal standard]. LCMS spectra were performed on Agilent 1260 LC equipped with a G6140 MSD detector (ESI mode). Elemental analysis was performed at the Analytical Laboratory of the V.P. Kukhar Institute of Bioorganic Chemistry and Petrochemistry of the NAS of Ukraine. Melting points were determined on the Boetius hot stage apparatus. Reaction progress was monitored by thin-layer chromatography.

Characteristics and spectral data of the synthesized compounds are provided in the SI.

Synthesis of compounds **1**, **2**, **4**, **11**, and **12** was described previously.³⁶

Methyl 7-(2-bromoethyl)-4-(methylamino)-7*H*-pyrrolo[2,3-*d*]pyrimidine-6-carboxylate (**3**) was synthesized according to the procedure described for compound **4**.³⁶

General procedure for the synthesis of compounds **5**, **6**, and **13**

A mixture of a pyrrolo[2,3-*d*]pyrimidine-6-carboxylate **3**, **4**, or **12** (1 mmol) and methylamine (40% aqueous solution) (4 mmol) in acetonitrile (1 mL) was stirred at room temperature for 12 h. The precipitate was filtered and recrystallized from methanol.

Methyl 7-(2-bromoethyl)-4-methoxy-7*H*-pyrrolo[2,3-*d*]pyrimidine-6-carboxylate (**7**)

A mixture of pyrrolo[2,3-*d*]pyrimidine-6-carboxylate **2** (5 mmol) and sodium methylate (5 mmol) in methanol (15 mL) was heated at 50–60 °C for 0.5 h. The reaction mixture was left at room temperature for 1 h. The resulting precipitate was filtered and recrystallized from methanol.

4-Methoxy-8,9-dihydropyrazino[1',2':1,5]pyrrolo[2,3-*d*]pyrimidin-6(7*H*)-one (**8**)

A mixture of compound **7** (2 mmol) and ammonium hydroxide solution (25%, 10 mmol) in acetonitrile (2 mL) was stirred at room temperature for 72 h. The reaction mixture was extracted with ethyl acetate, and the solvent was evaporated under reduced pressure. The resulting product was purified by crystallization from methanol.



4-Methoxy-7-methyl-8,9-dihydropyrazino[1',2':1,5]pyrrolo[2,3-*d*]pyrimidin-6(7*H*)-one (9)

A mixture of pyrrolo[2,3-*d*]pyrimidine-6-carboxylate 7 (3 mmol) and methylamine (2 M in methanol) (20 mL) was refluxed for 1 h. The solvent was evaporated under reduced pressure. The resulting product was purified by crystallization from methanol.

General procedure for the synthesis of compounds 10, 15, 17, 21, 24, 25, 27, and 32

A mixture of the appropriate starting material 9, 14, 16, 20, 23, 24, 26, or 31 (3 mmol) and ammonium acetate (15 mmol) was heated at 110–115 °C for 0.5–2 h (monitored by TLC). The reaction mixture was cooled and diluted with water (10 mL). The precipitate was filtered, washed with water, and recrystallized from the appropriate solvent.

General procedure for the synthesis of compounds 14 and 16

A mixture of pyrrolo[2,3-*d*]pyrimidine 1 (10 mmol), bromoacetal (40 mmol), and Cs₂CO₃ (40 mmol) in acetonitrile (25 mL) was refluxed for 72 h. The precipitate was filtered, and the solvent was evaporated under reduced pressure. The obtained residue was treated with boiling hexane. The solvent was evaporated, and dimethylamine (40% aqueous solution, 3 mL) was added to the residue. The reaction mixture was stirred at room temperature for 12 h. The product 16 was filtered and recrystallized from 2-propanol. To obtain compound 14, the residue was heated for 0.5 h at 50–60 °C with sodium methylate in methanol.

General procedure for *N*-methylation

A mixture of the appropriate starting material 1, 17, 21, 24, 29 or 32 (1 mmol), methyl iodide or chloroacetone (in case of compound 1) (2 mmol), and K₂CO₃ (2 mmol) in dimethylformamide (10 mL) was stirred at room temperature for 24 h. Water (20 mL) was added to the reaction mixture. The precipitate was filtered, washed with water, and dried. The obtained compounds 18, 19, 22, 26, 30, and 33 did not require further purification.

General procedure for the synthesis of compounds 20 and 23

A mixture of pyrrolo[2,3-*d*]pyrimidine-6-carboxylate 19 (3 mmol) and dimethylamine (2 M in methanol, 20 mL) or sodium methylate (3 mmol) in methanol (10 mL) was heated at 50–60 °C for 0.5 h. The reaction mixture was left at room temperature for 0.5 h. The resulting precipitate was filtered and recrystallized from methanol.

7,8-Dimethyl-4-(methylamino)pyrazino[1',2':1,5]pyrrolo[2,3-*d*]pyrimidin-6(7*H*)-one (28)

A mixture of compound 26 (1 mmol) and dimethylamine (40% aqueous solution, 5 mmol) in acetonitrile (2 mL) was stirred at room temperature for 36 h. The precipitate was filtered and recrystallized from a methanol/DMF mixture.

3-Methyl-8-methylene-8,9-dihydro-4*H*-pyrimido[5',4':4,5]pyrrolo[2,1-*c*][1,4]oxazine-4,6(3*H*)-dione (31)

A mixture of compound 30 (3 mmol) and anhydrous sodium acetate (6 mmol) in dimethylformamide (10 mL) was heated at 90 °C for 1 h. The reaction mixture was cooled and diluted with water (10 mL) after 1 h. The precipitate was filtered, washed with water, and recrystallized from a methanol/DMF mixture.

Acetylcholinesterase inhibition assay

Acetylcholinesterase from *Electrophorus electricus* (electric eel) was purchased from Sigma-Aldrich. The synthesized compounds were evaluated for their AChE inhibitory activity using modified Ellman's method.³⁹ The tested compounds were dissolved in DMSO. The total volume of the reaction mixture was 2 mL and contained 25 mM phosphate buffer (pH 7.4), inhibitor, enzyme, and 1% DMSO. The solution was thermostated for 5 min at 25 °C. Then DTNB was added for the detection of AChE activity. The reaction was started by adding *S*-acetylthiocholine iodide. The concentrations of DTNB and the substrate in the final volume of the reaction mixture were 1 mM and 0.1 mM, respectively. The activity of AChE was monitored spectrophotometrically at 412 nm by measuring the formation of 5-thio-2-nitrobenzoate after reaction of DTNB with thiocholine generated from the *S*-acetylthiocholine iodide by the enzyme. Donepezil and tacrine were used as reference compounds. The IC₅₀ values represent the concentrations of compounds that reduce enzyme activity by 50% at the substrate concentration of 0.1 mM. The IC₅₀ values were determined from dose-dependent curves obtained by plotting the percentage of remaining enzyme activity *versus* the logarithm of inhibitor concentration. The results were presented as mean ± standard deviation of three independent series of experiments.

Molecular docking

The crystal structure of hAChE with co-crystallized tacrine molecule at the anionic subsite of the catalytic site with PDB code 7XN1⁴³ was downloaded from the RCSB Protein Data Bank (<http://www.rcsb.org>).⁴⁸ Before performing docking calculations, the ligands, water molecules, and subunit B were removed from the downloaded file. The file containing subunit A was opened in AutoDockTools 1.5.6,⁴⁹ hydrogens were added, Gasteiger charges were assigned, and the structure was saved in PDBQT format. The structure of compound 22 was drawn using Marvin Sketch and saved in MOL2 format. The geometry was then optimized with the MMFF94 s force field in Avogadro.⁵⁰ Subsequently, the MOL2 file was opened in AutoDockTools 1.5.6 and converted to PDBQT format, preserving the assigned charges. Docking calculations were performed using AutoDock Vina.⁴⁰ Blind docking calculation was carried out using the whole surface of the subunit A. The grid box size was set to 80 with *x*, *y*, and *z* grid center coordinates of 53.992, −32.624, and −28.740, respectively. The grid box size was set to 15 with *x*, *y*, and *z* grid center coordinates of 48.178, −40.077, and −30.751 for ligand docking to the catalytic site. The redocking of the



tacrine molecule into the catalytic site was carried out for validation according to the docking protocol. The RMSD of the heavy atoms between the re-docked pose and the co-crystallized ligand was 0.57 Å. Discovery Studio 3.5 visualizer (Accelrys, San Diego, USA) was used for analysis and visualization of the docking and molecular dynamics results.

Molecular dynamics

To investigate the obtained binding modes of compound **22** and tacrine at the catalytic site, molecular dynamics simulations were performed using the NAMD 2.14 software package.⁵¹ To add the missing loop (Glu491-Ala497) to the protein structure of the complexes, a homology model was built with the help of the SWISS-MODEL server,⁵² using the amino acid sequence of human acetylcholinesterase (UniProt⁵³ entry P22303) and the PDB crystal structure with code 7XN1 as a template. The PROPKA method,⁵⁴ implemented in the PDB2PQR software,⁵⁵ was used to verify and correct the protonation states of amino acid residues at pH 7.4, which agree with *in vitro* study conditions. According to these calculations, Glu202 and His447 were represented in the MD simulations as Glh202 and Hid447, respectively.

The structure of hAChE was parameterized using the Amber ff14SB force field,⁵⁶ while parameterizations of the compound **22** and tacrine were carried out by ACPYPE software⁵⁷ using the generalized AMBER force field (GAFF)⁵⁸ with AM1-BCC charge method. The enzyme–inhibitor complexes were prepared by the LEaP module of AmberTools22. The enzyme–ligand complexes were solvated using the TIP3P water model in a box having dimensions 92.9 Å × 81.3 Å × 104.4 Å (total van der Waals box size), with a minimum distance of 12 Å between the amino acids and the edge of the water box. The sodium ions were added to the model systems to neutralize.

Before starting the production MD simulation, the model systems were energy minimized, heated, and equilibrated. Minimization was performed for 100 ps, keeping heavy atoms fixed to enable water molecules to spread correctly throughout the system. Periodic boundary conditions were employed alongside the particle mesh Ewald (PME) method, using a PME grid spacing of 1 Å and a tolerance of 1×10^{-6} . The simulations were conducted with a time step of 1 fs. Then, minimization for 100 ps was carried out without any atomic restraints. Subsequently, the system was heated from 0 K to 298.15 K over 50 ps at a rate of 0.007 K per step within the NVT ensemble. Equilibration was performed for 100 ps under NVT conditions and for 1 ns under NPT conditions. Temperature and pressure were controlled at 298.15 K and 1 atm (≈ 1.01325 bar) using Langevin thermostat and barostat methods, with damping coefficient, piston period, and piston decay set to 1 ps^{-1} , 50 fs, and 25 fs, respectively. The production molecular dynamics simulations were performed in the NPT ensemble for 20 ns, saving frames every 250 steps, resulting in a total of 80 000 frames. The trajectory files were subsequently down-sampled to 2000 frames using VMD version 1.9.3 REF. 59 and then analysed for root mean square deviation (RMSD), root mean square fluctuation

(RMSF), radius of gyration, and solvent-accessible surface area (SASA).

All the calculations and preparations described above, except the MD simulation, were performed in the conda environment.

MM/GBSA calculation

Free binding energies of compound **22** and tacrine at the CAS were calculated using MM-PBSA.py⁶⁰ available in AmberTools22. The calculation was performed using the last 1000 frames of the 2000-frame trajectory for each complex, with a sampling interval of 5 frames. The ionic strength was set to 0, and other parameters were set to default.

Drug-likeness evaluation

Assessment of physicochemical parameters, as well as pharmacokinetic and toxicity properties, was conducted by SwissADME (<https://www.swissadme.ch/>) and Deep-PK (<https://biosig.lab.uq.edu.au/deeppk/>). Canonical SMILES of the pyrazino[1',2':1,5]pyrrolo[2,3-*d*]pyrimidine derivatives were generated and entered into the list of SMILES section of SwissADME or saved in a txt format and loaded into Deep-PK. In the obtained results, particular attention was given to the analysis of compliance of the physicochemical parameters of the compounds with Lipinski's rule of five.⁴⁶ In the case of the ADMET properties, the intestinal absorption, blood–brain barrier penetration, and hepatotoxicity were selected.

Cytotoxicity assay on HepG2 cell line

HepG2 (ACC 180) cell line was provided by DSMZ, Germany. Cells were cultured in DMEM Hg medium containing 10% fetal bovine serum, 2 mM GlutaMax, 100 units per mL penicillin, and 100 $\mu\text{g mL}^{-1}$ streptomycin. Cells were maintained in the logarithmic growth phase at 37 °C in a humidified atmosphere containing 5% CO₂. Before plating, the cells were washed with DPBS and trypsinized with TrypLE solution. The appropriate volume of culture medium was placed in a flask to stop trypsinization. Cells were centrifuged, resuspended, stained with Trypan Blue, and counted using a counting chamber. The appropriate volumes of the cell suspensions were placed in the falcon tube containing the assay medium. HepG2 cells at 5000 cells per well density were seeded in sterile 384-well plates (Greiner Bio-One, Cat# 781091) in 60 μL /well and covered with sterile transparent seals. Plates were left overnight in a humidified atmosphere at 37 °C and 5% CO₂ for adaptation and adherence. The appropriate cell concentrations correspond to 30–35% of confluence before incubation with drugs. Cytotoxicity for the test compound was assessed at the final concentrations ranging from 0.005 μM to 100.0 μM (10 points, 3-fold serial dilutions). Incubation was performed for 48 hours in a humidified atmosphere at 37 °C and 5% CO₂. The final DMSO concentration in the assay was 0.5%. Then resazurin (50 μM final concentration) was added and incubated for 3 hours in a humidified atmosphere at 37 °C and 5% CO₂. The presence of resorufin was quantified by measuring fluorescence Ex – 555 nm, Em – 585 nm, cut-off 570, bottom read. The



concentration–response relationship was analyzed using a four-parameter logistic (4 PL) model.

Conclusions

In summary, eighteen pyrazino[1',2':1,5]pyrrolo[2,3-*d*]pyrimidines were designed and synthesized as potential tacrine-like AChE inhibitors. A new method for the synthesis of 8-methyl-substituted pyrazino[1',2':1,5]pyrrolo[2,3-*d*]pyrimidine derivatives was developed. *In vitro* evaluation showed that sixteen target compounds inhibited AChE in the micromolar range. Replacement of a dihydropyrazine ring with a pyrazine one and introduction of methyl groups at positions 7 and 8 of the pyrazino[1',2':1,5]pyrrolo[2,3-*d*]pyrimidine core resulted in a significant improvement in the inhibitory activity. Among the tested compounds, 4-(dimethylamino)-7,8-dimethylpyrazino[1',2':1,5]pyrrolo[2,3-*d*]pyrimidin-6(7*H*)-one (**22**) was the most potent AChE inhibitor with an IC₅₀ value of 0.22 ± 0.02 μM. Kinetic studies of compound **22** confirmed mixed-type inhibition. Like tacrine, the inhibitor showed strong π–π stacking interactions with Trp86 in the CAS of hAChE. *In silico* analysis suggested that **22** has an ADMET profile similar to that of tacrine. In addition, **22** demonstrates moderate cytotoxicity against the HepG2 cell line. Overall, the obtained results highlight pyrazino[1',2':1,5]pyrrolo[2,3-*d*]pyrimidine as a promising scaffold for the development of novel AChE inhibitors.

Author contributions

Conceptualization, L. V. Muzychka, O. B. Smolii, A. I. Vovk; synthesis of compounds, L. V. Muzychka, O. B. Smolii; bioactivity studies, O. V. Muzychka, O. L. Kobzar; writing – review and editing, L. V. Muzychka, O. V. Muzychka, O. L. Kobzar, A. I. Vovk, O. B. Smolii.

Conflicts of interest

There are no conflicts to declare.

Data availability

The data supporting this article have been included as part of the supplementary information (SI). Supplementary information is available. See DOI: <https://doi.org/10.1039/d5ra06700f>.

Acknowledgements

This work was supported by the National Academy of Sciences of Ukraine (projects 0125U000356 and 0125U000355). We are grateful to Liana Dmytrovska and Dr Petro Borysko (Enamine) for evaluating the *in vitro* cytotoxicity in HepG2 cells and to Inna Sokolenko for her help with manuscript preparation. The authors also thank the brave defenders of Ukraine, whose service allowed us to continue our scientific work and made this publication possible.

Notes and references

- 1 A. E. Abdallah, *RSC Adv.*, 2024, **14**, 11057–11088.
- 2 A. Sharma, S. Rudrawar, S. B. Bharate and H. R. Jadhav, *RSC Med. Chem.*, 2024, **16**, 652–693.
- 3 H. Xing, S. Yue, R. Qin, X. Du, Y. Wu, D. Zhangsun and S. Luo, *Int. J. Mol. Sci.*, 2025, **26**, 3905.
- 4 J. Marco-Contelles and M. J. Oset-Gasque, *Chem.-Biol. Interact.*, 2025, **413**, 111497.
- 5 L. C. Llanes, I. Kuehlewein, I. V. França, L. V. da Silva and J. W. da Cruz Junior, *Curr. Med. Chem.*, 2023, **30**, 701–724.
- 6 A. Sobha, A. Ganapathy, S. Mohan, N. Madhusoodanan, A. D. Babysulochana, K. Alaganandan and S. B. Somappa, *Eur. J. Med. Chem. Rep.*, 2024, **12**, 100237.
- 7 P. Arora, S. R. Swati, S. Jha, S. Gupta and S. Kumar, *Mol. Divers.*, 2025, **29**, 5367–5396.
- 8 S.-C. Peitzika and E. Pontiki, *Molecules*, 2023, **28**, 1084.
- 9 N. V. Mehta, A. Kapadia, M. Khambete and A. Abhyankar, *ChemBioChem*, 2025, **26**, e202500053.
- 10 S. M. Gupta, A. Behera, N. K. Jain, A. Tripathi, D. Rishipathak, S. Singh, N. Ahemad, M. Erol and D. Kumar, *RSC Adv.*, 2023, **13**, 26344–26356.
- 11 H. D. Nguyen and M. S. Kim, *Comput. Biol. Chem.*, 2023, **104**, 107872.
- 12 H. D. Nguyen and M. S. Kim, *J. Biomol. Struct. Dyn.*, 2024, **42**, 7128–7149.
- 13 M. A. Kale and M. Faisal, *Curr. Drug Res. Rev.*, 2025, **17**, 266–281.
- 14 F. Tok, *Chem. Biodivers.*, 2025, **22**, e202402837.
- 15 R. J. Obaid, N. Naeem, E. U. Mughal, M. M. Al-Rooqi, A. Sadiq, R. S. Jassas, Z. Moussa and S. A. Ahmed, *RSC Adv.*, 2022, **12**, 19764–19855.
- 16 O. M. Waly, K. M. Saad, H. I. El-Subbagh, S. M. Bayomi and M. A. Ghaly, *Eur. J. Med. Chem.*, 2022, **231**, 114152.
- 17 A. Dorababu, *Eur. J. Pharmacol.*, 2022, **920**, 174847.
- 18 N. Puranik and M. Song, *Neurol. Int.*, 2025, **17**, 26.
- 19 S. Mitra, M. Muni, N. J. Shawon, R. Das, T. B. Emran, R. Sharma, D. Chandran, F. Islam, M. J. Hossain, S. Z. Safi and S. H. Sweilam, *Oxid. Med. Cell Longev.*, 2022, **2022**, 7252882.
- 20 B. Sameem, M. Saedi, M. Mahdavi and A. Shafiee, *Eur. J. Med. Chem.*, 2017, **128**, 332–345.
- 21 M. Przybyłowska, S. Kowalski, K. Dzierzbicka and I. Inkielewicz-Stepniak, *Curr. Neuropharmacol.*, 2019, **17**, 472–490.
- 22 I. I. Jevtić, R. V. Suručić, G. Tovilović-Kovačević, N. Zogović, S. V. Kostić-Rajačić, D. B. Andrić and J. Z. Penjišević, *Bioorg. Med. Chem.*, 2024, **101**, 117649.
- 23 A. Babu, R. Chandran, S. Meleveetil, D. Vijayan, S. Kenchaiah, A. Khade, G. Zyryanov and N. J. Muthipeedika, *J. Mol. Struct.*, 2025, **1330**, 141479.
- 24 S. Fares, W. M. El Husseiny, K. B. Selim and M. A. M. Massoud, *ACS Omega*, 2023, **8**, 26012–26034.
- 25 S. Šegan, M. Mosić, V. Šukalović and I. Jevtić, *J. Chromatogr. B*, 2025, **1253**, 124481.
- 26 B. Svobodova, Z. Moravcova, A. Misiachna, G. Novakova, A. Marek, V. Finger and J. Korabecny, *Eur. J. Med. Chem.*, 2025, **292**, 117678.



- 27 Y. Zeng, L. Nie, L. Liu, K. Bozorov and J. Zhao, *J. Heterocycl. Chem.*, 2024, **61**, 1542–1553.
- 28 J. Zhang, Y. Li, J. D. Shao, G. Wei, N. Y. Zhang, K. K. Zhu, K. M. Wang, C. S. Jiang and J. H. Wang, *Mol. Divers.*, 2025, DOI: [10.1007/s11030-025-11354-9](https://doi.org/10.1007/s11030-025-11354-9).
- 29 E. A. Fayed, S. A. El-Sebaey, M. A. Ebrahim, K. Abu-Elfotuh, R. El-Sayed Mansour, E. K. Mohamed, A. M. E. Hamdan, F. T. Al-Subaie, G. S. Albalawi, T. M. Albalawi, A. M. Hamdan, A. A. Mohammed and T. M. Ramsis, *Eur. J. Med. Chem.*, 2025, **284**, 117201.
- 30 Y. G. Kappenberg, P. A. Nogara, F. S. Stefanello, C. P. Delgado, J. B. T. Rocha, N. Zanatta, M. A. P. Martins and H. G. Bonacorso, *Bioorg. Chem.*, 2023, **139**, 106704.
- 31 D. Turgunov, L. Nie, A. Nasrullaev, Z. Murtazaeva, B. Wang, D. Kholmurodova, R. Kuryazov, J. Zhao, K. Bozorov and H. A. Aisa, *Molecules*, 2025, **30**, 2791.
- 32 Y. Zeng, Z. Chen, Z. Yang, F. Yuan, L. Nie and C. Niu, *Mol. Divers.*, 2025, **29**, 3915–3931.
- 33 B. Kuzu and Y. Demir, *Arch. Biochem. Biophys.*, 2025, **771**, 110504.
- 34 A. Samadi, C. Valderas, C. de los Ríos, A. Bastida, M. Chioua, L. González-Lafuente, I. Colmena, L. Gandía, A. Romero, L. Del Barrio, M. D. Martín-de-Saavedra, M. G. López, M. Villarroya and J. Marco-Contelles, *Bioorg. Med. Chem.*, 2011, **19**, 122–133.
- 35 L. Jalili-Baleh, H. Nadri, A. Moradi, S. N. A. Bukhari, M. Shakibaie, M. Jafari, M. Golshani, F. Homayouni Moghadam, L. Firoozpour, A. Asadipour, S. Emami, M. Khoobi and A. Foroumadi, *Eur. J. Med. Chem.*, 2017, **139**, 280–289.
- 36 L. Muzychka, O. Muzychka and O. Smolii, *Chem. Biodivers.*, 2025, **22**, e202401874.
- 37 I. O. Yaremchuk, L. V. Muzychka, O. B. Smolii, O. V. Kucher and S. V. Shishkina, *Tetrahedron Lett.*, 2018, **59**, 442–444.
- 38 L. V. Muzychka, I. O. Yaremchuk, E. V. Verves and O. B. Smolii, *Chem. Heterocycl. Comp.*, 2019, **55**, 397–400.
- 39 G. L. Ellman, K. D. Courtney, V. Andress and R. M. Featherstone, *Biochem. Pharmacol.*, 1961, **7**, 88–95.
- 40 O. Trott and A. J. Olson, *J. Comp. Chem.*, 2010, **31**, 455–461.
- 41 A. Ganeshpurkar, R. Singh, S. Shivhare, Divya, D. Kumar, G. Gutti, R. Singh, A. Kumar and S. K. Singh, *Mol. Divers.*, 2022, **26**, 1455–1479.
- 42 M. F. Reynoso-Garcia, D. E. Nicolas-Alvarez, A. Y. Tenorio-Barajas and A. Reyes-Chaparro, *Int. J. Mol. Sci.*, 2025, **26**, 3781.
- 43 K. V. Dileep, I. Kentaro, M.-T. Chiemi, K.-N. Mutsuko, Y. Mayumi, H. Kazuharu, S. Mikako and K. Y. J. Zhang, *Int. J. Biol. Macromol.*, 2022, **15**, 172–181.
- 44 A. Daina, O. Michielin and V. Zoete, *Sci. Rep.*, 2017, **7**, 42717.
- 45 Y. Myung, A. G. de Sá and D. B. Ascher, *Nucleic Acids Res.*, 2024, **52**, W469–W475.
- 46 C. A. Lipinski, F. Lombardo, B. W. Dominy and P. J. Feeney, *Adv. Drug Deliv. Rev.*, 1997, **23**, 3–25.
- 47 D. E. Clark, *Drug Discov. Today*, 2003, **8**, 927–933.
- 48 H. M. Berman, J. Westbrook, Z. Feng, G. Gilliland, T. N. Bhat, H. Weissig, I. N. Shindyalov and P. E. Bourne, *Nucleic Acids Res.*, 2000, **28**, 235–242.
- 49 G. M. Morris, R. Huey, W. Lindstrom, M. F. Sanner, R. K. Belew, D. S. Goodsell and A. J. Olson, *J. Comp. Chem.*, 2009, **30**, 2785–2791.
- 50 M. D. Hanwell, D. E. Curtis and D. C. Lonie, *J. Cheminformatics*, 2012, **4**, 4–17.
- 51 J. C. Phillips, D. J. Hardy, J. D. C. Maia, J. E. Stone, J. V. Ribeiro, R. C. Bernardi, R. Buch, G. Fiorin, J. Henin, W. Jiang, R. McGreevy, M. C. R. Melo, B. K. Radak, R. D. Skeel, A. Singharoy, Y. Wang, B. Roux, A. Aksimentiev, Z. Luthey-Schulten, L. V. Kale, K. Schulten, C. Chipot and E. Tajkhorshid, *J. Chem. Phys.*, 2020, **153**, 044130.
- 52 A. Waterhouse, M. Bertoni, S. Bienert, G. Studer, G. Tauriello, R. Gumienny, F. T. Heer, T. A. P. de Beer, C. Rempfer, L. Bordoli, R. Lepore and T. Schwede, *Nucleic Acids Res.*, 2018, **46**, W296–W303.
- 53 The Uniprot Consortium, UniProt: the universal Protein knowledgebase in 2025, *Nucleic Acids Res.*, 2025, **53**, D609–D617.
- 54 H. Li, A. D. Robertson and J. H. Jensen, *Proteins*, 2005, **61**, 704–721.
- 55 T. Dolinsky, P. Czodrowski, H. Li, J. E. Nielsen, J. H. Jensen, G. Klebe and N. A. Baker, *Nucleic Acids Res.*, 2007, **35**, W522–W525.
- 56 J. A. Maier, C. Martinez, K. Kasavajhala, L. Wickstrom, K. E. Hauser and C. Simmerling, *J. Chem. Theory Comput.*, 2015, **11**, 3696–3713.
- 57 A. W. Sousa da Silva and W. F. Vranken, *BMC Res. Notes.*, 2012, **5**, 367.
- 58 J. Wang, R. M. Wolf, J. W. Caldwell, P. A. Kollman and D. A. Case, *J. Comput. Chem.*, 2004, **25**, 1157–1174.
- 59 W. Humphrey, A. Dalke and K. Schulten, *J. Mol. Graphics.*, 1996, **14**, 33–38.
- 60 B. R. Miller, T. D. McGee, J. M. Swails, N. Homeyer, H. Gohlke and A. E. Roitberg, *J. Chem. Theory Comput.*, 2012, **8**, 3314–3321.

